Earth and Planetary Science Letters 389 (2014) 1–13

Contents lists available at ScienceDirect

Earth and Planetary Science Letters

www.elsevier.com/locate/epsl

Slow wavespeeds and fluid overpressure in a region of shallow geodetic locking and slow slip, Hikurangi subduction margin, New Zealand

Dan Bassett [a,*], Rupert Sutherland [b], Stuart Henrys [b]

[a] University of Oxford, South Parks Road, Oxford, UK
[b] GNS Science, PO Box 30368, Lower Hutt 5040, New Zealand

ARTICLE INFO

Article history:
Received 30 April 2013
Received in revised form 9 December 2013
Accepted 13 December 2013
Available online xxxx
Editor: P. Shearer

Keywords:
slow slip
pore-pressure
seismic refraction
petroleum

ABSTRACT

Travel times recorded onshore from active-source marine seismic surveys were used to determine Hikurangi forearc wavespeeds. Ray-path midpoints sample forearc crust above the shallow (<10–12 km) subduction thrust. The southern region is locked to c. 30 km depth, exhibits slow slip at 30-45 km depth, and is similar to other subduction zones. Our 1D southern model has a rapid increase in seismic velocity (V_p) from the seabed to 4 km depth, consistent with rapidly-deposited clastic sediments, and near-constant $V_p = 5.0 \pm 0.2$ km/s at depths of 4–10 km within the forearc. The northern region has slow-slip events at shallow depths of c. 5–15 km, beneath the volume sampled by our analysis. Average travel times at offsets of 20–80 km are >1 s more than at equivalent offsets in the south, and V_p increases with depth within the forearc from 3.5 ± 0.1 km/s at 4 km depth to 4.5 ± 0.2 km/s at 10 km depth. We interpret the low wavespeeds in terms of compaction disequilibrium and compare seismic inferences of anomalously-high porosity (>10%) with hydrostatic reference compaction models to show effective stress is low in both the north (27 ± 10 Mpa) and south (36 ± 14 MPa). In the south, pore space and conduits have a high chance of being localized on faults or sand layers, the wedge is clearly compressionally critical, and we suggest the higher seismic velocities recorded primarily reflect higher effective stress levels transmitted through the rock framework. The observed wedge geometry and our estimate of fluid pressure within the wedge ($\lambda = 0.87 \pm 0.05$) suggest a weak overpressured subduction thrust. In the north, we suggest high fluid pressure is maintained by a large fluid inventory from subducting sediment, a pore-space geometry characterized by pervasively-fractured rock and mudstone, and a lower mean stress due to its stable and non-critical wedge geometry. We consider both end-member assumptions of convergent and tensile failure, the latter of which reveals the possibility of near-lithostatic fluid pressure on the north Hikurangi subduction interface, although this remains unproven. Our observations are consistent with high fluid pressures encountered in petroleum wells at depths <3 km and we observe a clear spatial correlation between the distribution of residual travel-times and the maximum depth of geodetic coupling and slow-slip. Our observations provide evidence for a causative link between high fluid pressure and anomalously-shallow slow slip events and depth of geodetic locking.

1. Introduction

Slow-slip events (SSEs) are identified from continuous geodetic observations as transient changes in surface velocity that last days to months and are inferred to be associated with slip on a fault at depth (Peng and Gomberg, 2010). They have been identified at almost every densely-instrumented subduction zone and are commonly interpreted as occurring within a transition between the up-dip strongly-coupled velocity-weakening and seismogenic portion of the subduction interface, and the down-dip steadily-creeping velocity-strengthening and aseismic region beneath (Schwartz and Rokosky, 2007). This frictional transition is characterized by a wide range of fault slip and seismogenic phenomena (Ide et al., 2007; Rubinstein et al., 2010; Wech and Creager, 2011), but what are the physical causes of this diverse behavior?

Several factors may control the occurrence of SSEs. Temperature controls the transition from friction to intra-crystalline plasticity as the dominant deformation mechanism (Sibson, 1982). Pore-fluid pressure controls effective stress and modulates a range of physical and chemical processes (Hubbert and Rubey, 1959). Variable frictional properties of fault zone materials, particularly phyllosilicate minerals, may also play an important role in modulating

* Corresponding author. Tel.: +44 01865 272046.
E-mail address: danielb@earth.ox.ac.uk (D. Bassett).

0012-821X/$ – see front matter
http://dx.doi.org/10.1016/j.epsl.2013.12.021

fault behavior (Moore and Rymer, 2007; Saffer and Marone, 2003; den Hartog and Spiers, 2013).

Most SSEs occur on subduction interfaces at the down-dip limit of the seismogenic zone at 30–45 km depth (Dragert et al., 2001; Larson et al., 2004; Obara et al., 2004; Ohta et al., 2004, 2006). The modeled temperature at this depth (c. 300–450 °C) coincides with a transition between brittle and ductile behavior in quartzofeldspathic rocks, and has led to the suggestion that this is the underlying cause of a locked–unlocked transition on subduction interfaces (Hyndman et al., 1997). This may be true in some places and is a widely-held explanation for the base of the seismogenic zone in continental crust (Sibson, 1982), but SSEs in New Zealand occur at temperatures <200 °C so thermally-induced crystal plasticity is unlikely to provide a universal explanation for global SSE phenomena (Peacock, 2009), and specifically cannot explain differences between the northern and southern Hikurangi margin (McCaffrey et al., 2008).

Elevated fluid pressures are expected in subduction zones, due to compaction and dehydration (e.g. Bray and Karig, 1985; Saffer and Tobin, 2011), and have been widely suggested as an explanation for the apparent anomalous weakness of subduction thrust faults (von Huene and Lee, 1982; Magee and Zoback, 1993; Tobin and Saffer, 2009; Scholz, 1998; Audet et al., 2009; Ito and Obara, 2006; Kodaira et al., 2004; Kitajima and Saffer, 2012; Sugioka et al., 2012). Observations that can be used to determine seismic wavespeed are the primary means to infer fluid pressure at depth; however it is challenging to make an accurate determination of wavespeed within the narrow fault zone, and the transformation between seismic velocity and effective stress state, in which pore pressure is intermediary, is uncertain and untested.

The Hikurangi subduction margin is ideal to address the question of what causes SSEs, because the southern region is geodetically locked to c. 30 km depth, has SSEs at c. 30–45 km depth, and in many respects appears similar to other subduction zones (Douglas et al., 2005; Wallace and Beavan, 2006; Beavan et al., 2007; Wallace et al., 2004). In contrast, the northern region appears to be freely-slipping beneath c. 15 km depth, and experiences SSEs in the depth range 5–15 km (Wallace et al., 2004). The detection of shallow SSEs suggests the onshore GPS network is sensitive to plate locking in offshore areas, although the uncertainty associated with geodetic locking distributions is expected to increase with distance from the coast. Geodetic observations also span a relatively short time period (10–20 yr) with respect to the likely period between large earthquakes, and the pattern of locking may evolve during the interseismic period (e.g. Wang et al., 2012), but inferences of short-term deformation and rotation rates are compatible with those made from geological observations since ~1.5 Ma (Nicol and Wallace, 2007). The geological materials, the basement rock and clastic sediments, are similar in both regions, but the margin normal convergence rate is a factor of two higher in the north and sediment thickness on the subducting Hikurangi Plateau exceeds 4 km in the south and is ~1 km in the north (Lewis et al., 1997; Wallace et al., 2004). What physical properties differ between the two regions, why, and how could this provide a viable explanation for the difference in slip style?

We use onshore–offshore wide-angle refraction data recorded during two seismic-reflection surveys to analyze the distribution of seismic wavespeeds within the shallow (<12 km depth) forearc wedges of the northern and southern parts of the Hikurangi subduction margin. We use empirical relations to relate seismic wavespeeds to porosity and effective stress, and consider wedge geometry and the burial history of subducted material. We find a striking difference between the northern and southern regions, with implications for understanding SSE behavior.

2. Regional setting

The Hikurangi margin exhibits significant along-strike transitions in margin structure, degree of interseismic coupling and depth distribution of slow slip events (see review by Wallace et al., 2009) (Fig. 1a). In the north, convergence is trench-normal at ~ 50 mm/yr (DeMets et al., 1994). In the south, convergence is highly oblique (>40°) at <40 mm/yr.

The northern Hikurangi margin is characterized by backarc extension, limited frontal accretion or tectonic erosion, and a steep frontal wedge taper of >10° (Barker et al., 2009; Barnes et al., 2010) (Fig. 1b). Campaign GPS data collected since the early 1990s show that this region has shallow (<15 km) interseismic coupling (Wallace et al., 2004). In contrast, the southern Hikurangi margin is characterized by regional accretion and upper plate contraction, shallow wedge taper ~5° (Fig. 1c), and considerably deeper (>30 km) interseismic coupling (Barker et al., 2009; Barnes and de Lepinay, 1997; Barnes et al., 2010; Wallace et al., 2004).

Sub-areal exposure of large portions of the Hikurangi fore-arc is causally related to the anomalous thickness (10–23 km) and buoyancy of the subducting plate, the Hikurangi Plateau (Davy and Wood, 1994). This enables geodetic measurements to be made near and above the shallow (<20 km) portions of the plate interface, and more than eight SSEs have been recorded along the Hikurangi margin since 2002, all of which are spatially consistent with the down-dip limit of geodetic locking (Fig. 3a).

SSEs recorded along the northern Hikurangi margin occur at depths of 5–15 km and are among the shallowest recorded on Earth (Douglas et al., 2005; Wallace and Beavan 2006, 2010; Beavan et al., 2007). Although shallow slow slip has also been recorded in Boso Peninsula (depth 10–20 km), Japan, and in Costa-Rica (depth 15–25 km), these events have been interpreted as nucleating from frictional transitions within the seismogenic zone (Schwartz and Rokosky, 2007) and northern Hikurangi SSEs are the shallowest associated with the down-dip edge of the geodetically defined locked zone.

Stress orientations computed from over 3000 focal mechanisms reveal trench-parallel orientations of maximum horizontal compressive stress (S_{Hmax}) in the north, in contrast to plate-motion-parallel S_{Hmax} orientations in the south (Townend et al., 2012). The boundary between these domains is located south of Hawke Bay (Fig. 1a). No large magnitude ($M_w \geqslant 7.5$) earthquakes have occurred on the Hikurangi subduction thrust in the last century, however, coseismic slip during two M_w 6.9–7.1 tsunami earthquakes near Gisborne in 1947 was limited to interface depths <20 km and is consistent with a shallow down-dip limit of the seismogenic zone along the northern Hikurangi margin (Downes et al., 2000; Doser and Webb, 2003).

Elevated pore fluid pressures within the weak geodetically-coupled northern Hikurangi margin are suggested by numerous mud volcanoes and directly measured in petroleum exploration wells near to the coast (Darby and Funnell, 2001; Sibson and Rowland, 2003). Receiver function analysis and 3D tomographic inversion of locally recorded earthquakes reveal high V_p/V_s and low Q_p near to the plate interface (Eberhart-Phillips et al., 2005; Reyners et al., 2006; Eberhart-Phillips et al., 2008). Low V_p/V_s and high Q_p is determined by tomographic studies in the southern region of deep interseismic locking and has been interpreted as regions of low permeability in the hanging wall (Eberhart-Phillips et al., 2008; Reyners and Eberhart-Phillips, 2009).

3. Pore-fluid pressure estimation and petrophysical models

Direct measurement of pore-pressure in boreholes is difficult, expensive, and can be dangerous in over-pressured tectonic

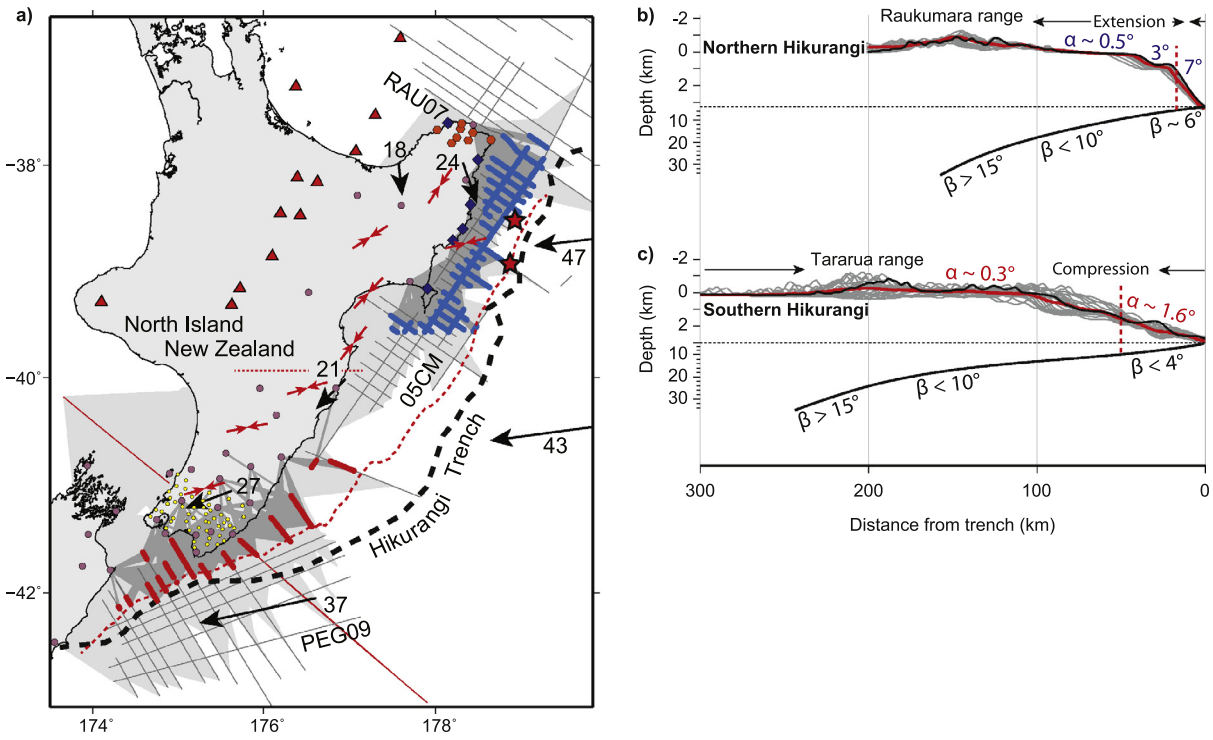

Fig. 1. (a) Tectonic setting of the Hikurangi subduction zone, New Zealand. Grey profiles display acquisition geometries of 05CM, RAU07 and PEG09 seismic reflection surveys. Black arrows show long-term motion of the Pacific plate (DeMets et al., 1994) and short-term (GPS) motion of the fore-arc (Wallace et al., 2004) relative to a fixed Australian plate. Red arrows show the axis of maximum horizontal compressive stress (S_{Hmax}) with the dotted red line marking the transition from trench parallel to plate-motion-parallel azimuths (Townend et al., 2012). Red triangles show locations of Holocene volcanic centres (de Ronde et al., 2001, 2007; Wright et al., 1996, 2006). Receivers were: GeoNet seismometers (pink circles), temporary deployments accompanying RAU07 (orange hexagons), 05CM (blue diamonds) and PEG09 (yellow circles). Seismic reflection shots are shown as grey lines. Red and blue profiles show shots used to constrain 1D models for the southern and northern Hikurangi margin respectively. The area of forearc sampled by these raypaths is shown dark grey. The raypaths of all other arrivals are shown light grey. Dashed red line marks the boundary between the back of the accretionary wedge and the front of a deforming buttress of Cretaceous and Paleogene rocks (Lewis et al., 1997; Barnes et al., 2010). Red stars show the locations of the 1947 tsunami earthquakes from Doser and Webb (2003). (b) Observed wedge geometry for the Northern Hikurangi margin. Trench-normal topographic profiles shown in grey with the ensemble average and profile in the centre of the margin segment shown in red and black respectively. Dashed red line marks the maximum landward extent of the accretionary wedge. Slab geometry in the centre of the segment is also shown in black (Williams et al., in press). The wedge geometry and margin sub-parallel direction of S_{Hmax} make critical wedge assumptions difficult to justify in this region. (c) As in (b) for the Southern Hikurangi margin. In addition to evidence of internal convergent failure, the consistency in wedge taper observed across the outer forearc suggests critical wedge assumptions may be valid in the Southern Hikurangi margin. (For interpretation of the references to color in this figure legend, the reader is referred to the web version of this article.)

settings. Drilling into a subduction thrust has only been attempted in a few settings and these efforts have been located near (typically <5 km) to a trench (e.g. Barbados: Moore et al., 1982; Moore and Tobin, 1997; SW Nankai: Moore et al., 2001; NE Nankai: Tobin et al., 2009; Saffer et al., 2009; Costa-Rica: McIntosh and Sen, 2000; Saffer, 2003), and only reach shallow depths (typically <1 km) beneath the seafloor that are unlikely to be representative of conditions where SSEs occur. Therefore, inference of fluid pressure at depth is required. These inferences have come from magnetotelluric and electromagnetic observations, detailed numerical modeling at many margins (e.g., Screaton et al., 1990; Wang, 1994; Bekins et al., 1995; Saffer and Bekins, 1998; Matmon and Bekins, 2006), and from large-scale studies of critical-taper and force balance (e.g., Kukowski et al., 2001; Davis and von Huene, 1987; Lallemand et al., 1994). Additional primary observations that can be used are either the travel-times of seismic arrivals or the amplitudes and phases of reflected arrivals.

The only tectonic environment for which a well-validated method of pore-fluid pressure estimation exists is that of sedimentary basins, because there are a large number of petroleum wells with direct pressure measurements. The primary remote observation method is active-source seismic-reflection, yielding average V_p over intervals (rock layers) and at impedance contrasts (reflective boundaries of layers). For a particular sediment type, seismic velocity is controlled by elastic moduli and density, and these are strongly negatively-correlated with porosity in most cases (Wyllie et al., 1956; Gardner et al., 1974; Eberhart-Phillips et al., 1989).

A relationship between porosity and effective stress and hence pore pressure is derived from the observation that burial compaction in sedimentary basins leads to a decrease in porosity (and bulk density increase) according to a predictable exponential function of depth in the hydrostatic case (Athy, 1930; Magara, 1978; Sclater and Christie, 1980). The form of this relation is largely controlled by sediment type although exact composition, thermal and burial/stress history and grain size are all important. If a rock has elevated fluid pressure resulting in compaction disequilibrium, and hence lower effective stress than expected for that burial depth, it appears 'under-compacted', with a positive porosity and concomitant negative V_p anomaly relative to the hydrostatic burial case. V_s decreases more rapidly than V_p with increased porosity, leading to an increase in V_p/V_s ratio in the under-compacted case (Eberhart-Phillips et al., 1989; Castagna et al., 1985).

To accurately estimate pore-pressure in a sedimentary basin, empirical calibration to the specific sediment characteristics and burial history is required. In addition, it is challenging to determine seismic wavespeed sufficiently precisely to make an inference of effective stress, because multi-channel seismic-reflection data typically have limited offset range (too small for refraction analysis), interval velocity calculation requires clear reflection events above and below the layer of interest (events may not exist), and reflection-amplitude analysis requires simplifying geological

assumptions (typically bimaterial planar layers greater than one wavelet thick) that may be unrealistic. However, a large number of surveys and boreholes have proven the value of the technique over many decades.

Seismic velocities in homogeneous elastic media are a function of elastic moduli and density (Gassmann, 1951). Elastic moduli are a function of the mixed mineral composition of grains, but water-filled or gas-filled porosity exerts the strongest influence on these parameters in the upper crust. The aspect ratios of pores in a petrophysical model strongly modulate the influence on seismic velocity, particularly if pores have high aspect ratios, such as in fractured rocks (Toksöz et al., 1976; Mavko et al., 1998).

Theoretical bounding velocities can be calculated for a specific value of porosity. The minimum seismic velocity, the Reuss lower bound (Reuss, 1929), is given by a model in which rock fragments are considered to be suspended within the fluid phase. The maximum seismic velocity, the Hashin–Shtrikman upper bound (Hashin and Shtrikman, 1963), is equivalent to a model in which the fluid-filled pores are trapped within shells of stiffer rock matrix.

For sedimentary rocks, empirical and theoretical relationships between porosity and seismic velocity have been developed (Wyllie et al., 1956; Nafe and Drake, 1957; Hamilton, 1978; Gardner et al., 1974). At high values of porosity (>25%), weakly-consolidated mudstones and sandstones have V_p just above the Reuss lower bound, consistent with their origin as a particle suspension. Compaction and failure under increasing effective stress during burial, combined with cementation and diagenesis, results in a stiffer rock that evolves towards the Hashin–Shtrikman upper bound.

The most widely used semi-empirical relation that relates porosity to seismic velocity in sedimentary basins is the "time-average" equation of Wyllie et al. (1956). This relationship is derived from consolidated sandstones with initial porosity of c. 30%. Raymer et al. (1980) improved the Wyllie relation by incorporating the heuristic concept of critical porosity, which defines the transition from a suspension to a continuous matrix (Nur et al., 1998), and developed three equations for different porosity ranges that apply to consolidated and cemented rock.

Using laboratory measurements, Eberhart-Phillips et al. (1989) developed an entirely empirical relationship between seismic velocity, effective pressure, porosity and clay content in water-saturated sandstones. This relation, and earlier relations of Han (1986), quantifies the significance of clay content when estimating porosity.

Erickson and Jarrard (1998) develop two empirical global velocity–porosity relationships that recognize the influence of burial and horizontal stresses on both compaction-related porosity loss and pressure-induced increases in inter-grain coupling. The first relationship is for normally-consolidated sediments (e.g. sedimentary basins) and the other is for highly-consolidated environments. The latter has been used widely in accretionary prism settings (e.g. Barbados, Erickson and Jarrard, 1999).

The Nafe and Drake curve (Ludwig et al., 1970) and Gardner's rule (Gardner et al., 1974) provide empirical relationships between velocity and density derived from a large range of common lithologies (not just sedimentary). These relations provide an estimate of bulk density from which porosity can be calculated assuming densities for grains (fully-compact rock) and the pore-volume.

4. Pore fluid pressure in subduction zones

Subduction zones are environments where large fluid pressure anomalies may exist, but there are three primary difficulties with understanding pore-fluid pressures in these settings. First, there is high variability of rock types and porosity–stress–velocity relationships, few samples to constrain rock properties, and so it is hard to justify the choice of a specific petrophysical model or empirical relationship. Second, the complex geological structures, expensive offshore–onshore logistics for experiments, and restricted distribution of earthquake hypocentres makes it challenging to image seismic velocity anomalies with high precision and resolution. Third, there is little or no observational ground truth to test estimated pore pressure or stress anomalies.

The issue is of broad interest and transforms from seismic velocity to effective stress have been used to estimate excess pore pressure in the vicinity of the décollement of several subduction zones (e.g. Barbados: Bangs et al., 1990; Hayward et al., 2003; Nankai: Tobin and Saffer, 2009). The influence of lateral tectonic stresses above the décollement on the effective stress that controls consolidation have been considered in a number of studies using either experientially or empirically derived calculations of principal stress magnitudes (Moore and Tobin, 1997), using a particular rock physics model (e.g. Tsuji et al., 2008); or using empirical relations calibrated by laboratory deformation tests on drill core samples (Kitajima and Saffer, 2012).

At the Nankai subduction zone in Japan, low velocities (V_p 2.7–3.2 km/s) resolved from multi-channel and wide-angle seismic surveys (Park et al., 2010) have been analyzed using locally-calibrated empirical relations between velocity, porosity (Hoffman and Tobin, 2004), and effective stress to infer high pore-fluid pressure (depth averaged Rubey–Hubbert ratio $\lambda = 0.51$–0.77) above the décollement (Kitajima and Saffer, 2012). The region of highest pore-fluid pressure is correlated with locations of very low frequency earthquakes (VLFEs) (Ito and Obara, 2006; Sugioka et al., 2012), providing evidence for a link between high pore-fluid pressure (low effective stress) and low-stress-drop slip phenomena such as VLFEs and SSEs (Kitajima and Saffer, 2012).

Elevated pore-fluid pressures inferred from high Poisson's ratios and high V_p/V_s have been linked with SSEs in Japan (Kodaira et al., 2004) and Episodic Tremor and Slip (ETS) in Cascadia (Audet et al., 2009). In these studies, however, inferred high pore-fluid pressures reside within the subducting slab rather than the overlying wedge, and are far less well constrained or understood than inferences made nearer the trench and at shallower depths in subduction zones. In Cascadia, Calvert et al. (2011) resolve lower seismic velocities within a >4 km thick band of reflectors overlying the subducting Juan de Fuca slab, which they interpret as subducted and underplated sediments. High electrical conductivity, high V_p/V_s and the correlation of non-volcanic tremor and SSEs with the low-velocity zone is interpreted as suggesting low effective stresses and high pore-fluid pressures within this volume. Analogous to observations made in Cascadia, in the southern Hikurangi margin, high V_p/V_s (>1.8) and low Q_p (<400) is resolved within a low-velocity prism, which is similarly interpreted as underplated material (Eberhart-Phillips et al., 2005; Henrys et al., 2013). This prism, however, is located up dip of the location of SSEs and the geodetically inferred locked–unlocked transition, and Henrys et al. (2013) suggest underplating of sediments alone may not be a strong discriminator of geodetic behavior. In contrast to the studies mentioned above where effective stress levels and pore-pressure are inferred from seismic and other geophysical observations but not estimated explicitly, placing bounds on these parameters is a key objective of this study.

5. Rock types, seismic velocity, and porosity at the Hikurangi margin

Torlesse Supergroup clastic sedimentary rocks were accreted and deformed at the Gondwana forearc during Mesozoic time, and were then overlain by, tectonically imbricated with, or underthrust by Cretaceous–Cenozoic chalks, mudstone, siltstone, and sandstone.

Torlesse Supergroup rocks are exposed onshore in eastern North Island and have been extensively sampled and geophysically studied in South Island. The greywacke composition and low-grade (regionally sub-greenschist) metamorphism of this terrane are described elsewhere (MacKinnon, 1983; Cox and Barrell, 2007). Laboratory analyses of Torlesse Supergroup samples under confining pressure show $V_p = 6.0 \pm 0.3$ km/s at 100–200 MPa (equivalent to 5–10 km depth) and 6.3 ± 0.3 km/s at 600 MPa (equivalent to 22 km depth) (Christensen and Okaya, 2007). These velocities are consistent with those resolved in situ by seismic surveys and earthquake tomography in eastern South Island, where $V_p = 5.9$–6.1 km/s at depths $\leqslant 15$ km (Davey et al., 1998; Leitner et al., 2001; Eberhart-Phillips and Bannister, 2002; van Avendonk et al., 2004).

At the southern Hikurangi margin, the presence of older (Permian–Triassic) Rakaia terrane Torlesse Supergroup has been linked with the deeper down-dip extent of geodetic locking. Although compositionally similar to younger Torlesse Supergroup rocks, this terrane is suggested to be impermeable and prevents fluid from crossing the plate interface and entering the overlying wedge (Reyners and Eberhart-Phillips, 2009). The surficial dip-parallel extent of this terrane is relatively small (typically <50 km) and is only sampled by a small proportion ($<2\%$) of the ray-paths we analyze in our study, because it lies mostly farther west. Torlesse Supergroup rocks in our study region are primarily Cretaceous Pahau terrane and compositional variability is expected to be low (Mortimer, 2004).

The subducting Hikurangi plateau is part of the Hikurangi–Manihiki–Ontong Java large igneous province, is 15–20 km thick with V_p 4.9–7.3 km/s (Scherwath et al., 2010; Bassett et al., 2010; Henrys et al., 2013), and is overlain by fine-grained Cretaceous and Paleogene deep-water sediments (Davy et al., 2008). Neogene sediment gravity flows and hemi-pelagic sediment thicken southward from ~1 km off northeastern North Island to ~6 km off northeastern South Island (Lewis et al., 1998; Barnes et al., 2010). Hemi-pelagic and localized canyon or slope-basin sedimentation also takes place across the trench-slope region. Neogene sediments have similar composition and are forming in a similar environment to that inferred for Mesozoic Torlesse Supergroup sediments.

It is unclear how much of the forearc wedge is composed of Torlesse basement terrane versus underplated and imbricated younger clastic materials (e.g. Fig. 12 of Bassett et al., 2010; Reyners et al., 1999; Eberhart-Phillips and Reyners, 1999; Eberhart-Phillips and Chadwick, 2002; Henrys et al., 2013).

6. Data and analysis

We analyzed seismic reflection surveys that acquired over 5000 line-km of multi-channel seismic-reflection (MCS) data along the Hikurangi margin since 2005 (see Supplementary material). During each survey, the GeoNet nationwide array was supplemented by temporary seismometers. Records of onshore arrivals of refracted and wide-angle-reflected seismic waves yield ray-paths that sample much of the Hikurangi fore-arc, subduction interface and subducting Hikurangi Plateau. Seismic energy is recorded at offsets as large as ~250 km and travel-times of over 1 million unique ray-paths are interpreted. Travel-times and offsets were corrected to remove the section of raypath through water. We restrict the analysis presented here to refracted arrivals confined to the northern and southern forearc wedges and analyze an offset range of 20–80 km with broad azimuthal coverage (Fig. 1a). We exclude shots from water depths >1600 m and arrivals with offset >80 km because these raypaths are not confined within the forearc wedge. The forearc near the trench is therefore not constrained (Figs. 1 and 3). All remaining observations have ray-paths entirely landward of the structural division separating the late Cenozoic frontal accretionary wedge beneath lower continental slope from a deforming foundation of pre-subduction, Cretaceous and Paleogene passive margin rocks and overlying Miocene – recent slope basins (Barnes et al., 2010; Division dashed in red in Figs. 1 and 3b).

Our primary goal is to evaluate if there is a resolvable difference in average forearc V_p between the northern and southern regions of the Hikurangi margin. Therefore, we aim to find the best average 1D velocity model with depth below the seabed and separately analyze the northern (05CM survey) and southern (PEG09 survey) regions. At depths $\leqslant 2$ km beneath the seabed, we use stacking velocities derived directly from reflection processing (05CM: Multiwave, 2005; PEG09: Geotrace, 2010; streamer length 10–12 km). At greater depths, we perform a least-squares optimization to fit offshore–onshore water-corrected travel times of turning rays within the forearc wedge. We identify this phase from its geometrical relationship to faster slab phases and wide-angle reflections on receiver gathers (an additional check on our shot location and limited-offset criterion).

We use a 2D finite-difference travel-time solver (Hole and Zelt, 1995), to calculate model travel-time as a function of offset, based on a simple 1D parameterization. We evaluate the sum of squared residual travel times as our metric of fit, and use a downhill simplex method to find the best-fitting parameters (see Supplementary material). We considered parameterizations of this problem with just 3 or 4 optimization nodes between 3 and 15 km depth. Our preferred (simplest) configuration is shown in Figs. 2b and 2d.

We chose the least number of parameters required to describe this problem, because the underlying question is a simple one: is there a resolvable difference between the velocity–depth functions, on average, between northern and southern regions? There is spatial variability within each region, revealed by scatter of travel-time residuals, but the number of ray paths is large, so standard errors of model parameters are relatively small (Fig. 2).

7. Results: velocity structure of forearc wedge

Our models reveal a contrast in velocity structure between the northern and southern Hikurangi margin that is prominent in the shallow (<10 km) fore-arc wedge, above the subduction thrust (Fig. 2).

Seismic-reflection stacking velocities, determined with typical maximum offsets of 8–12 km, reveal similar shallow (0–2 km bsf) velocity gradients of ~0.6 km s^{-1} km^{-1}. The gradient in the southern Hikurangi margin is offset to slightly higher values than in the north, possibly reflecting higher sand content. This shallow velocity structure is typical for sediment burial compaction.

The velocity gradient at the northern Hikurangi margin shallows to a near-constant 0.33 km s^{-1} km^{-1} at 2–10 km depth, but the velocity gradient in the south steepens to 0.75 km s^{-1} km^{-1} resulting in a 1.3 ± 0.1 km s^{-1} difference between south and north at 4 km depth (Fig. 2). The near-constant velocity (~5.0 km s^{-1}) observed at 4–10 km depth in the south results in convergence between velocity models beyond 10 km depth. At depths >10 km, uncertainty envelopes overlap between northern and southern models (Fig. 2b and d). The velocity of ~6.5 km s^{-1} at 15 km depth is consistent with the subducting Hikurangi Plateau (e.g. Scherwath et al., 2010; Henrys et al., 2013), but histograms of subducting slab depth (Williams et al., in press) at ray-path midpoints show that the maximum depth to which our models can be confidently interpreted is 10 km in the north and 12 km in the south (Figs. 2b and 2d).

A spatial analysis of difference in velocity structure between the northern and southern Hikurangi margin was undertaken by fitting a polynomial to all travel-time observations as a function of offset. We plotted the residual travel-time for each raypath at the source–receiver midpoint, and then spatially averaged over a 25 km radius

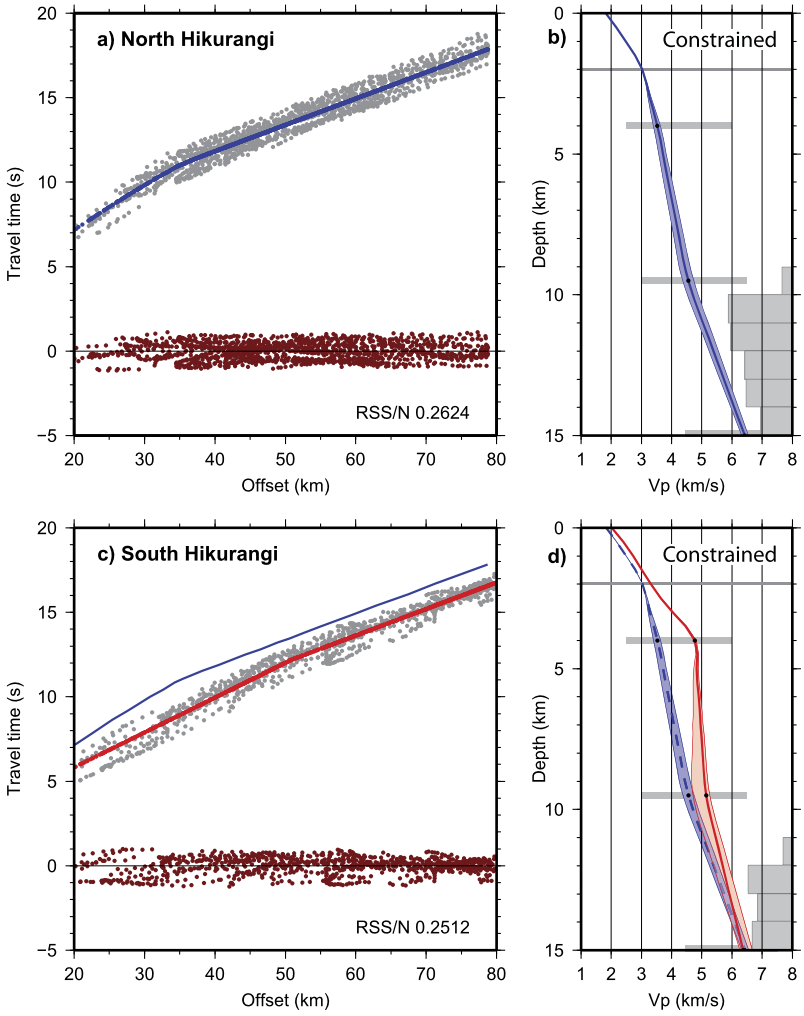

Fig. 2. (a) Water-corrected travel-times picks from the Northern Hikurangi margin and the travel-time offset curve generated for the 1D velocity model best fitting these observations. Residuals from this curve are displayed in red. The best fitting 1D velocity model is shown in (b). The light blue region represents the uncertainty in this model (95% confidence, see Supplementary material). Thin grey bars show the maximum range over which optimization nodes could vary during uncertainty analysis (see Supplementary material). Subducting slab depth (Williams et al., in press) at ray-path midpoints is shown as a histogram. (c) As in (a) for the Southern Hikurangi margin. Blue profile shows the travel-time – offset curve for the northern Hikurangi margin from (a) for comparison. Note the similar gradients in the travel-time offset curves at offsets greater than 50 km. (d) As in (b) for the Southern Hikurangi margin. Dashed blue profile shows the 1D model and uncertainty envelope for the northern Hikurangi margin from (b) for comparison. (For interpretation of the references to color in this figure legend, the reader is referred to the web version of this article.)

(Fig. 3b). Residual travel-times are calculated using data corrected for water depth. The approximate equality between the number of observations from north and south and the wide range of ray azimuths preclude significant population bias in this analysis.

Travel-times at specific offset in the northern Hikurangi margin are ∼1.5 s greater (implying lower V_p) than those in the southern region (Fig. 3b). The greatest residual travel-times are observed north of Gisborne, and are correlated with a south-to-north transition in the depth of interseismic coupling inferred from GPS data to even shallower levels near the trench, but it is likely that significant uncertainties are associated with locking distributions here (Wallace et al., 2004). Residual travel-times offshore Raukumara Peninsula are higher than those south of Gisborne, and inland of the Poverty indentation, Mahia Peninsula appears as a region of lower residual travel-times and may represent a local relative velocity high (Pedley et al., 2010).

South of Hawke Bay, Cape Turnagain is coincident with a sharp ∼0.7 s reduction in residual travel-times and separates the transitional and gradually-reducing residual travel-times in the central margin from the regionally-low (<-0.3 s) southern segment. The location of this boundary is spatially-correlated with a north-to-south increase in the depth of interseismic coupling from <15 km to >30 km (Wallace et al., 2004).

The lowest residual travel-times (implying fastest V_p) are observed beneath Wellington and southern Wairarapa. The sharp southern boundary of this low is dotted in Figs. 3a and 3b and is spatially correlated with a clockwise rotation of the trench to an azimuth near-parallel with the plate-convergence vector. This boundary is also coincident with the southern flank of a saddle in the depth of interseismic coupling. This saddle is interpreted by Wallace et al. (2004) as the likely southern termination of a large subduction thrust rupture and we suggest it may mark the eastward continuation of a regional terrane boundary that is well defined in north eastern South Island and suggested to truncate the Rakaia Terrane through Cook Straight (see Fig. 2 of Mortimer, 2004; Reyners and Eberhart-Phillips, 2009).

8. Forearc rocks: pore volume and geometry

The primary control on seismic velocity of the Hikurangi forearc is likely to be pore volume. We use empirical relationships between velocity and porosity and we assume that the pore volume

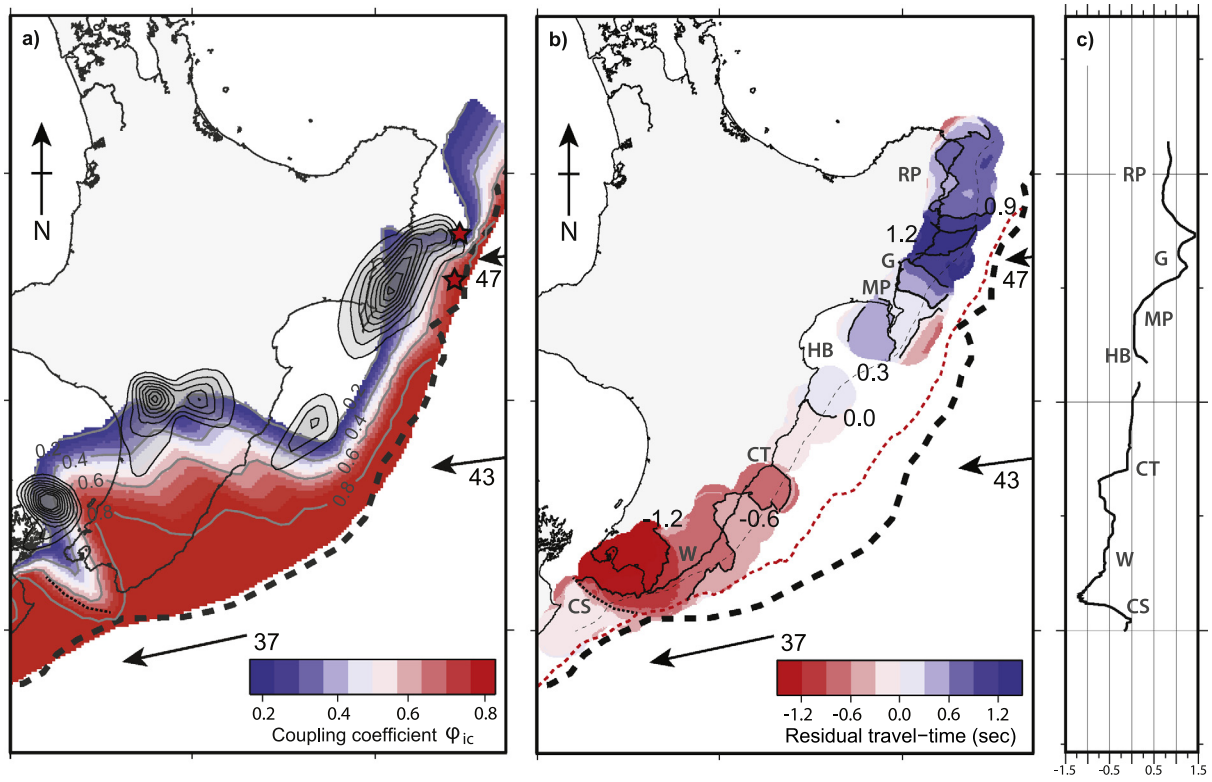

Fig. 3. (a) Slip rate deficit distribution at the plate interface (Wallace et al., 2004). Red regions are where the plate interfaced is geodetically locked. Black contours show cumulative slip (mm) in slow-slip events (SSEs) during 2002–2012, outer most contour at 100 mm then at 50 mm increments (Wallace et al., 2012). Red stars show the locations of the 1947 tsunami earthquakes from Doser and Webb (2003). Dotted black line shows the possible Rakaia terrane boundary interpreted from travel-time anomalies in Cook Straight. (b) Travel-time anomalies for the Hikurangi subduction fore-arc. Anomalies are calculated as residuals from a polynomial fit to all water-corrected travel-times. Note the strong correlation at Cape Turnagain between the sudden reduction in residual travel-times and the factor >2 increase in the depth of interseismic coupling. Dashed red line marks the boundary between the back of the accretionary wedge and the front of a deforming buttress of Cretaceous and Paleogene rocks (Lewis et al., 1997; Barnes et al., 2010). Locations discussed in text are Raukumara Peninsula (RP), Gisbourne (G), Mahia Peninsula (MP), Hawke Bay (HB), Cape Turnagain (CT), Wairarapa (W) and Cook Straight (CS). (c) Profile showing residual travel-time anomalies along strike. The location of this profile follows the 100 m depth contour and is displayed in fine black dash in (b). Note the sharp reduction in residual travel-times at Cape Turnagain and the sharp increase in residual travel-times in Cook Straight. (For interpretation of the references to color in this figure legend, the reader is referred to the web version of this article.)

geometries of rocks along Hikurangi margin are sufficiently similar to make this comparison meaningful.

To estimate porosity we apply the polynomial regression of Brocher (2005) to the Nafe and Drake relationship presented graphically by Ludwig et al. (1970), and the lithology-specific (sandstone) polynomial form of the Gardner V_p–ρ relationship (Castagna et al., 1993).

Porosity in the north is close to the hydrostatic reference porosity curve ($\phi_0 = 0.5$ and $\beta = 3$, Athy, 1930; Rubey and Hubbert, 1959) to a depth of 2 km before shallowing to a near linear gradient between $\phi = 25\%$ at 2 km depth and $\phi = 10\%$ at 10 km depth (Fig. 4a). Relative to the porosity–depth profile in the south, both the Nafe–Drake and Gardner relations suggest that porosity within the northern Hikurangi forearc wedge is >5% higher between 3 and 10 km depth and >8% higher between 3.5 and 6 km depth.

Also displayed in Fig. 4 are ϕ – depth curves calculated using the high consolidation relation of Erickson and Jarrard (1998), and the relation of Eberhart-Phillips et al. (1989) for the hydrostatic case ($\rho_{grain} = 2.74$ g/cm^3 clay content = 0.2). The latter relation predicts a steeper compaction curve in both north and south with higher porosity at depths <3–4 km and lower porosity at greater depth, possibly reflecting the assumption of hydrostatic fluid pressures. The high-consolidation relation of Erickson and Jarrard (1998) predicts a porosity–depth curve close to the convergent wedge hydrostatic reference curve in the south but in the north is significantly offset from both reference porosity curves by >10% between 3–9 km depth.

Uncertainty envelopes calculated around the Nafe and Drake curve incorporate uncertainty in the fully-compact rock velocity and hence particle density (6.0 ± 0.3 km/s between 5 and 10 km depth, Christensen and Okaya, 2007) and the original uncertainty associated with 1D velocity models (Figs. 2b and 2d). Additional sources of uncertainty include those associated with the velocity–density transformation, a significant proportion of which relate to contact quality of grains and the aspect ratio of pore-spaces on transforms between V_p and ρ. Effects of the latter have been estimated and incorporated into rock physics models (e.g. Takei, 2002; Tsuji et al., 2008), however, the absence of constraints on pore-geometry, relative proportions, exact composition and consolidation behavior of materials, and the large area over which our average velocity models are calculated make it difficult to justify the application of a more complex petrophysical model in this study.

9. Effective stress

The primary reason for lower porosity in the southern region is, we suggest, because there are higher mean stress levels at equivalent depths. This is caused by some combination of (1) higher stress levels transmitted through the rock framework, and (2) lower pore-fluid pressure. We assume that lithology and cementation/lithification state are similar in the north and south (or that V_p is not sensitive to lithology), it is the magnitude of maximum principal effective stress that limits rock compaction, and we follow a similar strategy to previous workers e.g. the Barbados subduction margin analysis of Moore and Tobin (1997).

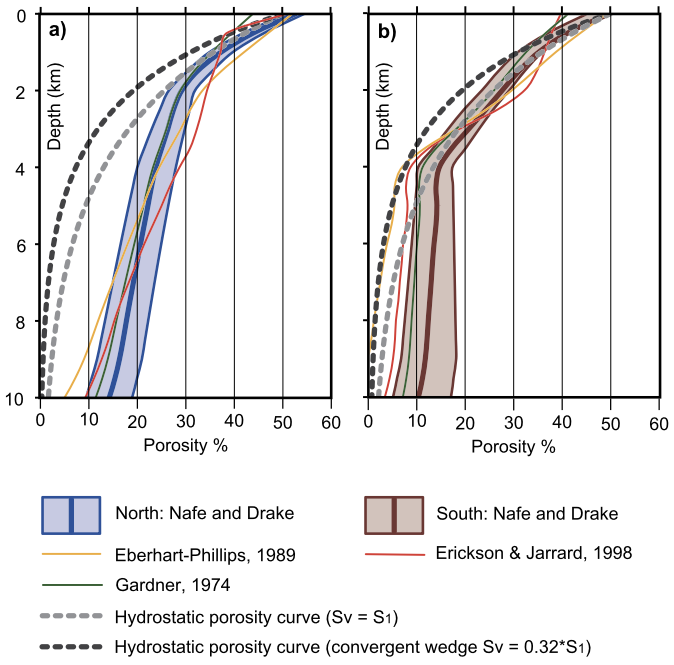

Fig. 4. Average porosity–depth profiles calculated for the (a) northern and (b) southern Hikurangi margin from 1D velocity models. Light grey dash shows a hydrostatic reference porosity curve ($\phi_0 = 0.5$ and $\beta = 3$) that assumes the vertical stress is close to the maximum stress. In reality, it may be much greater and the dark grey dash shows the hydrostatic reference porosity curve for the convergent wedge solution with $S_v = 0.32 \cdot S_1$ (equivalent to an angle of incohesive internal friction of 31° or coefficient of friction $\mu = 0.6$). This curve indicates both regions are significantly under-compacted and porosity in the North is at least 15% higher than estimated for hydrostatic burial. Uncertainty envelopes calculated around the Nafe and Drake curve incorporate uncertainty in grain density and seismic velocity. We estimate porosity uncertainty to be ±5% in the north (>2 km depth) and ±7% in the south (>4 km depth).

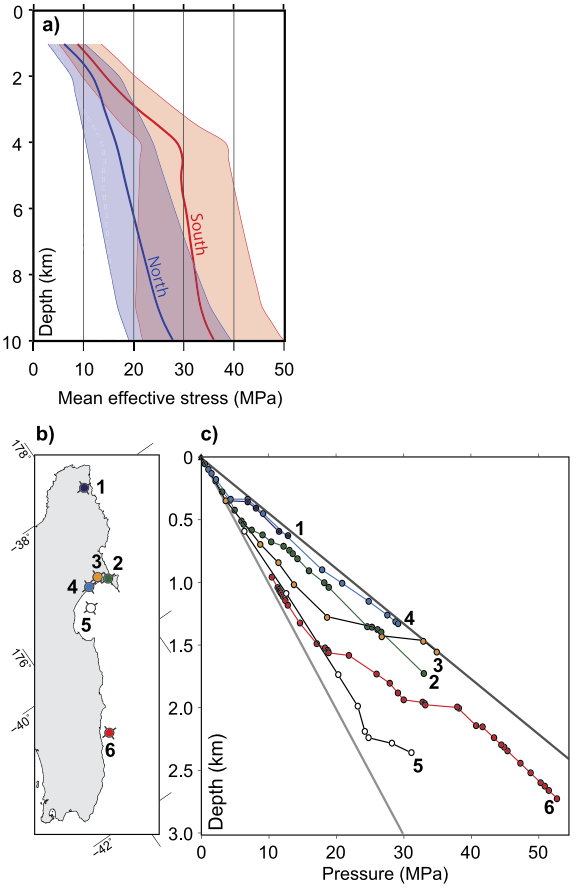

Fig. 5. (a) Mean effective stress for the northern (blue) and southern (red) Hikurangi margin. We estimate K_0 pore-fluid pressure ratios within the wedge (λ_w) of 0.73 ± 0.11 in the north and 0.63 ± 0.11 in the south. Assuming thrust failure ($\mu_w = 0.6$), λ_w increases to 0.89 ± 0.04 in the north and 0.87 ± 0.05 in the south. Uncertainty envelopes include uncertainty in modeled porosity (Fig. 4), reference porosity (ϕ_0) and compaction length scale (β). b) Locations and c) fluid pressures estimated from mud weights in petroleum exploration wells (adapted from Darby and Funnell, 2001). Wells shown are 1 – Rotokautuku-1; 2 – Opoutama-1; 3 – Mangaone-1; 4 – Kauhauroa-3; 5 – Hawke Bay-1; 6 – Titihaoa-1. (For interpretation of the references to color in this figure legend, the reader is referred to the web version of this article.)

We first estimate effective stress (Fig. 5) by comparing inferred porosity against a reference exponential compaction model derived from empirical hydrostatic uniaxial loading (vertical effective stress is the maximum principal effective stress, $\sigma_v = \sigma_1$), as measured in sedimentary basins and laboratory experiments

$$\Phi = \Phi_0 \exp(-\beta \sigma_1) \quad (1)$$

where Φ_0 is the initial porosity and β is the rock compaction coefficient (Athy, 1930; Terzaghi and Peck, 1948; Rubey and Hubbert, 1959).

There is large uncertainty associated with the rock compaction coefficient in this study, because Hikurangi forearc rocks have not been sampled and tested directly. We assume quartzo-feldspathic rock grain strengths at the Hikurangi margin are similar to those found in nearby Taranaki Basin, where the sediment compaction length scale is 2.5 ± 0.5 km, and initial porosity is 0.50 ± 0.05 (Funnell et al., 1996). We converted this to a compaction effective stress coefficient of 25 ± 5 MPa, assuming hydrostatic conditions and lithostatic maximum stress in Taranaki Basin.

The compaction length scale we obtain from fitting near-surface data at the Hikurangi margin (0–2 km depth in the north, and 0–4 km depth in the south) is 3.0 ± 0.2 km, which is only slightly greater than is found in Taranaki. Fluid overpressure at the Hikurangi margin, however, can be significant in wells at depths as shallow as 0.5 km in the north and 2.0 km in the south, and is observed in most wells at 2–4 km depth (Fig. 5) (Darby and Funnell, 2001), confirming the likely role of fluid overpressure in maintaining anomalous porosity.

In the northern Hikurangi forearc region we calculate from our seismic velocity inference of porosity that the effective stress at 10 km depth is 27 ± 10 MPa. In the southern Hikurangi forearc, we calculate the effective stress at 10 km depth is 36 ± 14 MPa (Fig. 5b). It is widely assumed that compaction is a function of the mean effective stress (i.e. Dvorkin et al., 1999), so that is the quantity that these values likely represent.

10. Absolute stress and fluid pressure

To calculate absolute mean stress and fluid pressure for any given value of mean effective stress, at least one additional constraint or assumption is required. In many sedimentary basins, this is commonly the uni-axial burial assumption, but horizontal tectonic stresses in a subduction forearc may be substantial in magnitude. We assume the ratio (R) of the maximum and minimum principle stresses is the same in the upper plate of subduction zones as in uniaxially compacting sedimentary basins, and that the material is isotropic of terms of stress–strain behavior and velocity.

We calculate the state of stress within the forearc using equations that describe a non-cohesive Coulomb wedge at failure everywhere (Davis et al., 1983; Dahlen, 1984). Horizontal effective stress during thrust failure is greater than vertical (lithostatic) effective stress. Uniform wedge geometry and extensive evidence for internal convergent failure suggests that critical wedge assumptions are justified for the outer-forearc of the southern Hikurangi

margin (Fig. 1c). We assume: a forearc coefficient of friction of $\mu = 0.6$; horizontal maximum principal effective stress (wedge solution gives plunge of 3° in the southern region); and hence the mean effective stress is a factor of 1.6 times the effective vertical (minimum) lithostatic stress.

The southern region has an average surface slope (α) of 1.6°, and a décollement dip (β) of 3.5° is estimated from seismic-reflection data. We estimate a mean effective stress of 36 ± 14 MPa at 10 km depth from our velocity model. The velocity model and failure criterion together implies a Hubbert–Rubey fluid pressure ratio at 10 km depth of $\lambda = 0.87 \pm 0.05$ where

$$\lambda = \frac{P_f - \rho_w g D}{|\sigma_z| - \rho_w g D}, \tag{2}$$

P_f is the pore fluid pressure ρ_w is the density of pore fluid, D is depth, and $|\sigma_z|$ is the magnitude of the vertical stress. The wedge solution yields a basal shear stress $\tau_b = 11 \pm 3$ MPa and basal fluid pressure ratio $\lambda_b = 0.93 \pm 0.02$, which implies a weak overpressured subduction thrust.

The frictional properties of Hikurangi forearc rocks are poorly known. Laboratory measurements of the frictional strength of materials from subduction zones includes siliceous clastics and metapelites with friction coefficients that range from 0.2–0.5 (Brown et al., 2003; Ikari et al., 2009; den Hartog et al., 2012; den Hartog and Spiers, 2013). These values are less than friction coefficients ($\mu = 0.6$–1.0) associated with internal friction angles of 30–45° (Byerlee, 1978), which are typical of crustal rocks, widely used in taper analyses, and are consistent with the orientation of observed thrust faults at the Hikurangi margin (Barker et al., 2009; Bell et al., 2010). Although direct measurement of friction coefficients have not been made from materials found at the Hikurangi margin, a discrepancy between direct friction measurements and the geometry of conjugate thrust faults is also observed in Nankai (Lallemand et al., 1994; Brown et al., 2003). The uncertainty in friction coefficient is significant and affects how much greater the maximum principal effective stress is above the minimum effective stress. This in turn affects the fluid pressure calculation derived from our inference of mean effective stress. For a coefficient of friction $\mu = 1.0$ a convergent solution for the southern margin at 10 km depth yields $\lambda = 0.92 \pm 0.03$, whereas $\mu = 0.2$ yields $\lambda = 0.79 \pm 0.07$.

The northern region wedge geometry and observations of forearc failure are less clearly appropriate for application of a critical wedge model. We estimate the mean effective stress in this region to be 27 ± 10 MPa at 10 km depth, implying $\lambda = 0.89 \pm 0.04$, assuming the convergent critical case with $\mu = 0.6$. The outer wedge (Fig. 1b) has a frontal section characterized by reverse faults, an average surface slope (α) of 7°, and a décollement dip (β) of <6°, and is not predicted to be stable unless $\lambda < 0.87$. However, our data primarily sample the inner part of the wedge, which has a much lower surface slope (α) of <1°, and décollement dip (β) of 6–10°, for which the convergent wedge solution implies $\tau_b = 12 \pm 4$ MPa and $\lambda_b = 0.93 \pm 0.02$. The composite wedge has α in the range 3–4° and β in the range 7–9°, which is close to the wedge stability criterion, and wedge stability requires only a slightly greater fluid pressure or lower friction coefficient on the plate interface beneath, with implied basal shear stress $\tau_b \approx 25$ MPa.

Failure within the wedge in the northern region is not clearly convergent. Although there is evidence for forearc reverse faulting on seismic sections, and from the 1931 Napier earthquake, the inner part of the wedge is characterized by a contemporary (last few decades) direction of maximum horizontal stress (S_{Hmax}) that is sub-parallel to the margin (Townend et al., 2012), rather than margin-normal as expected for a critically-tapered compressional wedge. In the Raukumara Peninsula, northern Hikurangi, Neogene rocks of the overlying plate have been normal-faulted (e.g. Thornley, 1996; Mazengarb, 1984), and trenchward extensional strain is also seen in the focal mechanisms of small earthquakes in the uppermost part of the overlying plate (Reyners and McGinty, 1999).

We consider the possibility that the upper plate is failing in tension in the northern region. In this case, the maximum principal stress is approximately the vertical stress, and the absolute levels of mean stress predicted at any given depth are lower. A friction coefficient of $\mu = 0.6$ and proximity-to-failure assumption yields $\lambda = 0.67 \pm 0.15$. The extensional critical wedge solutions for the range of geometrical and frictional parameters discussed predict low values (<10 MPa) of basal shear stress, values very close to zero, or even values with opposite sign to that expected. The results imply that, if there was extensional failure within the wedge, then the plate interface must have near-lithostatic fluid pressures or be composed of very weak materials.

In summary, effective stress levels we estimate are <20% of the lithostatic stress at 10 km depth, so both regions must have a high degree of fluid overpressure ($\lambda > 0.5$, even at extensional failure). Convergent failure implies a horizontal maximum stress greater than the vertical stress, higher mean stress, and hence a higher degree of fluid overpressure ($\lambda > 0.85$). If the materials at convergent failure have low intrinsic strength (e.g. $\mu = 0.2$) then a lower degree of overpressure is implied but the absolute level must still be high ($\lambda > 0.7$ for convergent failure). There is abundant evidence for convergent failure within the southern wedge, but the northern wedge may be closer to extensional failure at present. Extensional wedge solutions for the geometry of the northern region imply low basal shear stress values (<10 MPa), and include the possibility of zero effective stress at the base. The tensile wedge solution represents an end-member and it seems most reasonable that the northern region has a stable non-critical wedge geometry that lies between tensile and convergent limits.

11. Discussion

We observe a clear spatial correlation between the distribution of residual-travel times and the maximum depth of geodetic coupling and SSEs.

The northern and southern margins are accreting sediment at different rates. The southern Hikurangi margin is actively accreting Neogene mud and silt with sand lenses. The mechanism of accretion is imbrication along stacked thrust faults, and there is a clear focusing of fluid seeps along these faults (Lewis and Marshall, 1996; Barnes and de Lépinay, 1997; Barnes et al., 2010). At the northern Hikurangi margin, a greater proportion of plate displacement is accommodated on the subduction thrust (Nicol et al., 2007). Much of the northern Hikurangi forearc is overlain offshore by weakly-deformed Miocene–Pliocene hemipelagic mudstones and silt-dominated slope basins up to 2 km thick. Different petrophysical models may be appropriate for each region and we suggest that pore spaces and conduits for fluids in the south have a higher chance of being localized on faults or sand layers than in the north.

Excess pore fluid pressure is related to the fluid inventory. Fluid input to the northern forearc at 5–15 km depth is likely to be higher than in the south for two reasons. First, margin normal convergence across the subduction interface is double in the north (Wallace et al., 2004). Second, the underthrusting/subducting sediment is primarily composed of Late Cretaceous and Paleogene sediment that is relatively uncompact and water-rich at the trench in the north, but has been compacted and partially-dewatered by burial beneath up to 6 km of Neogene sediment in the south. These arguments are supported by global observations and modeling studies of links between sediment thickness, con-

vergence rate, wedge taper and pore pressure (Bekins and Dreiss, 1992; Clift and Vannuchi, 2004; Saffer and Bekins, 2006)

Our observations of low seismic velocities reflect compaction disequilibrium in both regions (e.g. Gibson, 1958; Swarbrick, 1997; von Huene and Lee, 1982; Bethke, 1986; Saffer and Tobin, 2011). We suggest a larger pore volume is maintained in the north by a greater fluid inventory from underthrusting/subducting sediment, a pore-space geometry that is characterized by pervasively-fractured rock and mudstone, rather than localized fault and sandstone channels, and a lower mean stress due to its stable and non-critical wedge geometry. Our inference of high fluid pressure within the northern forearc wedge is consistent with magnetotelluric data (Heise et al., 2012) but is not consistent with earlier mechanical arguments for hydrostatic conditions (Fagereng and Ellis, 2009). We suggest that higher seismic velocities in the south are mainly the result of higher effective stress levels transmitted through the rock framework and wedge failure is manifest as pervasive thrust faults that offset young strata.

12. Conclusion

We address the issue of robust seismic velocity determination within the forearc wedge in two ways. Firstly, we use rays with a wide range of azimuths and offsets that turn entirely within the forearc wedge, as interpreted from the geometry of arrivals on receiver gathers of many shots (Fig. 1). Secondly, we solve for the least number of parameters required to uniquely determine the magnitude and gradient of velocity within the forearc wedge. This approach precisely determines average values within a region, but ignores local variability (Fig. 2).

We find a striking correlation between travel-time delays and along-strike changes in locking behavior on the subduction interface (Fig. 3). Shallow locking and SSE phenomena are correlated with slower wavespeeds within the forearc wedge. We interpret the slow wavespeeds in both the northern and southern regions in terms of compaction disequilibrium, elevated pore-fluid pressure, and relatively-low effective stress.

The southern Hikurangi margin has near-constant $V_p = 5.0 \pm 0.2$ km/s at depths of 4–10 km, which is low compared to most crustal values, but comparable to that inferred at other subduction zones (Tobin and Saffer, 2009; Kitajima and Saffer, 2012). We estimate a mean effective stress of 36 ± 14 MPa at 10 km depth from our velocity model and the critical wedge assumption of convergent failure. We estimate a Hubbert–Rubey fluid pressure ratio at 10 km depth of $\lambda = 0.87 \pm 0.05$, a basal shear stress $\tau_b = 11 \pm 3$ MPa, and basal fluid pressure ratio $\lambda_b = 0.93 \pm 0.02$. Our calculations indicate a weak over-pressured subduction thrust.

The northern Hikurangi forearc wedge has extremely low V_p values, as compared to other subduction margins or equivalent rocks found elsewhere in New Zealand. Average travel times at offsets of 20–80 km are >1 s more than at equivalent offsets in the south, and V_p increases with depth within the forearc from 3.5 ± 0.1 km/s at 4 km depth to 4.5 ± 0.2 km/s at 10 km depth. Observations from petroleum wells support the hypothesis that high fluid pressures exist. The wedge geometry and criticality condition are less certain in the north, and conflicting evidence does not support the conclusion that the wedge is at critical failure everywhere. Convergent-failure end-member solutions yield similar results to the southern region, but tensile-failure end-member solutions reveal the possibility of near-lithostatic fluid pressures on the north Hikurangi subduction interface. Although unproven, we speculate that this may be a primary cause of shallow SSE phenomena and propose that this hydrological condition is a primary control on the dramatic change in along-strike locking behavior on the subduction interface.

Acknowledgements

Funds for data acquisition and analysis were provided by the New Zealand Government and by Marsden Fund project GNS0902 from the Royal Society of New Zealand This work has benefited from discussion with John Townend, and we thank the editor Peter Shearer, Lisa McNeill, and Demian Saffer for helpful and constructive comments that considerably improved the manuscript.

Appendix A. Supplementary material

Supplementary material related to this article can be found online at http://dx.doi.org/10.1016/j.epsl.2013.12.021.

References

Athy, L.F., 1930. Density, porosity, and compaction of sedimentary rocks. Am. Assoc. Pet. Geol. Bull. 14, 1–22.

Audet, P., Bostock, M.G., Christensen, N.I., Peacock, S.M., 2009. Seismic evidence for overpressured subducted oceanic crust and megathrust fault sealing. Nature 457, 76–78.

Bangs, N.L., Westbrook, G.K., Ladd, J., Buhl, P., 1990. Seismic velocities from the Barbados Ridge complex: Indicators of high pore fluid pressures in an accretionary complex. J. Geophys. Res. 95 (B6), 8767–8782. http://dx.doi.org/10.1029/JB095iB06p08767.

Barker, D., Sutherland, R., Henrys, S., Bannister, S., 2009. Geometry of the Hikurangi subduction thrust and upper plate, North Island, New Zealand. Geochem. Geophys. Geosyst. 10, Q02007. http://dx.doi.org/10.1029/2008GC002153.

Barnes, P.M., de Lepinay, B.M., 1997. Rates and mechanics of rapid frontal accretion along the very obliquely convergent southern Hikurangi margin, New Zealand. J. Geophys. Res. 102, 24,931–24,952.

Barnes, P.M., et al., 2010. Tectonic and geological framework for gas hydrates and cold seeps on the Hikurangi subduction margin, New Zealand. Mar. Geol. 272, 26–48.

Bassett, D., Sutherland, R., Henrys, S., Stern, T., Sherwath, M., Benson, A., Toulmin, S., Henderson, M., 2010. Three-dimensional velocity structure of the northern Hikurangi margin, Raukumara, New Zealand: implications for the growth of continental crust by subduction erosion and tectonic underplating. Geochem. Geophys. Geosyst. 11, Q10013. http://dx.doi.org/10.1029/2010GC003137.

Beavan, J., Wallace, L., Douglas, A., Fletcher, H., 2007. Slow slip events on the Hikurangi subduction interface, New Zealand. In: Tregoning, P., Rizos, C. (Eds.), Monitoring and Understanding a Dynamic Planet With Geodetic and Oceanographic Tools. IAG Symposium, vol. 130. Cairns, Australia, 22–26 August 2005. Springer, Berlin, pp. 438–444.

Bekins, B.A., Dreiss, S.J., 1992. A simplified analysis of parameters controlling dewatering in accretionary prisms. Earth Planet. Sci. Lett. 109, 275–287.

Bekins, B.A., McCaffrey, A., Dreiss, S.J., 1995. Episodic and constant flow models for the origin of low-chloride waters in a modern accretionary complex. Water Resour. Res. 31, 3205–3215.

Bell, R., Sutherland, R., Barker, D.H.N., Henrys, S., Bannister, S., Wallace, L., Beavan, J., 2010. Seismic reflection character of the Hikurangi subduction interface, New Zealand, in the region of repeated Gisborne slow slip events. Geophys. J. Int. 180, 34–48. http://dx.doi.org/10.1111/j.1365-246X.2009.04401.x.

Bethke, C.M., 1986. Inverse hydrogeologic analysis of the distribution and origin of Gulf Coast-type geopressured zones. J. Geophys. Res. 91, 6535–6545.

Bray, C.J., Karig, D.E., 1985. Porosity of sediments in accretionary prisms and some implications for dewatering processes. J. Geophys. Res. 90, 768–778.

Brocher, T.M., 2005. Empirical relations between elastic wavespeeds and density in the Earth's crust. Bull. Seismol. Soc. Am. 95 (6), 2081–2092. http://dx.doi.org/10.1785/0120050077.

Brown, K.M., Kopf, A., Underwood, M.B., Weinberger, J.L., 2003. Compositional and fluid pressure controls on the state of stress on the Nankai subduction thrust: A weak plate boundary. Earth Planet. Sci. Lett. 214, 589–603.

Byerlee, J., 1978. Friction of rocks. Pure Appl. Geophys. 116, 615–626.

Calvert, A.J., Preston, L.A., Farahbod, A.M., 2011. Sedimentary underplating at the Cascadia mantle-wedge corner revealed by seismic imaging. Nat. Geosci. 4. http://dx.doi.org/10.1038/NGEO1195.

Castagna, J.P., Batzle, M.L., Eastwood, R.L., 1985. Relationship between compressional-wave and shear-wave velocities in clastic silicate rocks. Geophysics 50 (4), 571–581.

Castagna, J.P., Batzle, M.L., Kan, T.K., 1993. Rock physics – The link between rock properties and AVO response. In: Castagna, J.P., Backus, M. (Eds.), Offset-dependent Reflectivity: Theory and Practice of AVO Analysis. In: Investigations in Geophysics, vol. 8, pp. 135–171.

Christensen, N., Okaya, D., 2007. Compressional and shear-wave velocities in South Island New Zealand rocks and their application to the interpretation of seismological models of the New Zealand crust. In: Okaya, D., et al. (Eds.),

A Continental Plate Boundary: Tectonics at South Island, New Zealand. In: Geophys. Monogr. Ser., vol. 175. AGU, Washington, DC, pp. 125–155.
Clift, P., Vannucchi, P., 2004. Controls on tectonic accretion versus erosion in subduction zones: Implications for the origin and recycling of the continental crust. Rev. Geophys. 42, RG2001. http://dx.doi.org/10.1029/2003RG000127.
Cox, S.C. Barrell, D.J.A., (compilers) 2007. Geology of the Aoraki Area, Institute of Geological and Nuclear Sciences 1:250,000 geological amp 15, 1 sheet + 71 pages. Lower Hutt, New Zealand, GNS Science.
Dahlen, F.A., 1984. Noncohesive critical Coulomb wedges: An exact solution. J. Geophys. Res. 89, 10125–10133.
Darby, D., Funnell, R.H., 2001. Overpressure associated with a convergent plate margin: East Coast Basin, New Zealand. Pet. Geosci. 7 (3), 291–299.
Davey, F., et al., 1998. Preliminary results from a geophysical study across a modern continent–continent collisional plate boundary – the Southern Alps, New Zealand. Tectonophysics 288, 221–235.
Davis, D.M., von Huene, R., 1987. Inferences on sediment strength and fault friction from structures at the Aleutian Trench. Geology 15, 517–522.
Davis, D.M., Suppe, J., Dahlen, F.A., 1983. Mechanics of fold-and-thrust belts and accretionary wedges. J. Geophys. Res. 88, 1153–1172.
Davy, B., Wood, R., 1994. Gravity and magnetic modeling of the Hikurangi Plateau. Mar. Geol. 118, 139–151. http://dx.doi.org/10.1016/0025-3227(94)90117-1.
Davy, B., Hoernle, K., Werner, R., 2008. Hikurangi Plateau: Crustal structure, rifted formation, and Gondwana subduction history. Geochem. Geophys. Geosyst. 9, Q07004. http://dx.doi.org/10.1029/2007GC001855.
de Ronde, C., Baker, E., Massoth, G., Lupton, J., Wright, I., Feely, R., Greene, R., 2001. Intra-oceanic subduction-related hydrothermal venting, Kermadec volcanic arc, New Zealand. Earth Planet. Sci. Lett. 193, 359–369. http://dx.doi.org/10.1016/S0012-821X(01)00534-9.
de Ronde, C., et al., 2007. Submarine hydrothermal activity along the mid-Kermadec Arc, New Zealand: Large-scale effects on venting. Geochem. Geophys. Geosyst. 8, Q07007. http://dx.doi.org/10.1029/2006GC001495.
DeMets, C., Gordon, R.G., Argus, D.F., Stein, S., 1994. Effect of recent revisions to the geomagnetic time scale on estimates of current plate motions. Geophys. Res. Lett. 21, 2191–2194. http://dx.doi.org/10.1029/94GL02118.
den Hartog, S.A.M., Spiers, C.J., 2013. Influence of subduction zone conditions and gouge composition on frictional slip stability of megathrust faults. Tectonophysics 600, 75–90.
den Hartog, S.A.M., Peach, C.J., De Winter, D.A.M., Spiers, C.J., Shimamoto, T., 2012. Frictional properties of megathrust fault gouges at low sliding velocities: new data on effects of normal stress and temperature. J. Struct. Geol. 38, 156–171.
Doser, D.I., Webb, T.H., 2003. Source parameters of large historical (1917–1961) earthquakes, North Island, New Zealand. Geophys. J. Int. 152, 795–832.
Douglas, A., Beavan, J., Wallace, L., Townend, J., 2005. Slow slip on the northern Hikurangi subduction interface, New Zealand. Geophys. Res. Lett. 32, L16305. http://dx.doi.org/10.1029/2005GL023607.
Downes, G.L., Webb, T.H., McSaveney, M., Darby, D., Doser, D., Chague-Goff, C., Barnett, A., 2000. The March 25 and May 17 1947 Gisborne earthquakes and tsunami: implication for tsunami hazard for east coast, North Island, New Zealand. In: Gusiakov, V.K., Levin, B.W., Yakovenko, O.I. (Eds.), Tsunami Risk Assessment Beyond 2000: Theory, Practice and Plans, Moscow, pp. 55–67.
Dragert, H., Wang, K., James, T., 2001. A silent slip event on the deeper Cascadia subduction interface. Science 292, 1525–1528.
Dvorkin, J., Manika, P., Sakai, A., Lavoie, D., 1999. Elasticity of marine sediments: Rocks physics modeling. Geophys. Res. Lett. 26 (12), 1781–1784.
Eberhart-Phillips, D., Bannister, S., 2002. Three-dimensional crustal structure in the Southern Alps region of New Zealand from inversion of local earthquake and active source data. J. Geophys. Res. 107 (B10), 2262. http://dx.doi.org/10.1029/2001JB000567.
Eberhart-Phillips, D., Chadwick, M., 2002. Three-dimensional attenuation model of the shallow Hikurangi subduction zone in the Raukumara Peninsula, New Zealand. J. Geophys. Res. 107 (B2), 2033. http://dx.doi.org/10.1029/2000JB000046.
Eberhart-Phillips, D., Reyners, M., 1999. Plate interface properties in the Northeast Hikurangi Subduction Zone, New Zealand, from converted seismic waves. Geophys. Res. Lett. 26 (16), 2565–2568. http://dx.doi.org/10.1029/1999GL900567.
Eberhart-Phillips, D., Han, D., Zoback, M., 1989. Empirical relationships among seismic velocity, effective pressure, porosity, and clay content in sandstone. Geophysics 54 (1), 82–89. http://dx.doi.org/10.1190/1.1442580.
Eberhart-Phillips, D., Reyners, M., Chadwick, M., Chiu, J.M., 2005. Crustal heterogeneity and subduction processes: 3-D V_p, V_p/V_s and Q in the southern North Island, New Zealand. Geophys. J. Int. 162, 270–288.
Eberhart-Phillips, D., Reyners, M., Chadwick, M., Stuart, G., 2008. Three-dimensional attenuation structure of the Hikurangi subduction zone in the central North Island, New Zealand. Geophys. J. Int. 174, 418–434.
Erickson, S.N., Jarrard, R.D., 1998. Velocity–porosity relationships for water-saturated siliciclastic sediments. J. Geophys. Res. 103, 30385–30406.
Erickson, S.N., Jarrard, R.D., 1999. Porosity-formation factor and porosity–velocity relationships in Barbados prism. J. Geophys. Res. 104 (B7), 15391–15407.
Fagereng, A., Ellis, S., 2009. On factors controlling the depth of interseismic coupling on the Hikurangi subduction interface, New Zealand. Earth Planet. Sci. Lett. 278, 120–130.
Funnell, R., et al., 1996. Thermal state of the Taranaki Basin, New Zealand. J. Geophys. Res., Solid Earth 101 (B11), 25197–25215.
Gardner, G.H.F., Gardner, L.W., Gregory, A.R., 1974. Formation of velocity and density – The diagnostic basics for stratigraphic traps. Geophysics 39, 770–780. http://dx.doi.org/10.1190/1.1440465.
Gassmann, F., 1951. Elastic waves through a packing of spheres. Geophysics 16, 673–685.
Geotrace, 2010. Pegasus, Bounty Trough, Great South Basin and Sahke Processing Report. Volume PR4279. Open File Petroleum Report, Wellington, New Zealand, pp. 1–19.
Gibson, R.E., 1958. The progress of consolidation in a clay layer increasing with time. Geotechnique 8, 171–182.
Hamilton, E.L., 1978. Sound velocity–density relations in sea-floor sediments and rocks. J. Acoust. Soc. Am. 634, 366–377.
Han, D., 1986. Effects of porosity and clay content on wave velocities in sandstones. Geophysics 51, 2093–2107.
Hashin, Z., Shtrikman, S., 1963. A variational approach to the elastic behavior multiphase minerals. J. Mech. Phys. Solids 11, 127–140.
Hayward, N., Westbrook, G.K., Peacock, S., 2003. Seismic velocity, anisotropy, and fluid pressure in the Barbados accretionary wedge from an offset vertical seismic profile with seabed sources. J. Geophys. Res. 108 (B11), 2515. http://dx.doi.org/10.1029/2001JB001638.
Heise, W., Caldwell, T.G., Hill, G.J., Bennie, S.L., Wallin, E., Bertrand, E.A., 2012. Magnetotelluric imaging of fluid processes at the subduction interface of the Hikurangi margin, New Zealand. Geophys. Res. Lett. 39 (4), L04308.
Henrys, S., et al., 2013. SAHKE Geophysical transect reveals crustal and subduction zone structure at the southern Hikurangi margin, New Zealand. Geochem. Geophys. Geosyst.
Hoffman, N.W., Tobin, H.J., 2004. An empirical relationship between velocity and porosity for underthrust sediments in the Nankai Trough accretionary prism. In: Proc. Ocean Drill. Program Sci. Results, vol. 190/196, pp. 1–23.
Hole, J.A., Zelt, B.C., 1995. 3-D finite-difference reflection traveltimes. Geophys. J. Int. 121, 427–434.
Hubbert, M.K., Rubey, W.W., 1959. Mechanics of fluid-filled porous solids and its application to overthrust faulting. Geol. Soc. Am. Bull. 70, 115–166. http://dx.doi.org/10.1130/0016-7606(1959)70(115:ROFPIM)2.0.CO.
Hyndman, R.D., Yamano, M., Oleskovich, D.A., 1997. The seismogenic zone of subduction thrust faults. Island Arc 6, 244–260.
Ide, S., Beroza, G.C., Shelly, D.R., Uchide, T., 2007. A scaling law for slow earthquakes. Nature 447 (7140), 76–79. http://dx.doi.org/10.1038/nature05780.
Ikari, M.J., Saffer, D.M., Marone, C., 2009. Frictional and hydrologic properties of clay rich fault gouge. J. Geophys. Res. 114, B05409.
Ito, Y., Obara, K., 2006. Dynamic deformation of the accretionary prism excites very low frequency earthquakes. Geophys. Res. Lett. 33, L02311. http://dx.doi.org/10.1029/2005GL025270.
Kitajima, H., Saffer, D.M., 2012. Elevated pore pressure and anomalously low stress in regions of low frequency earthquakes along the Nankai Trough subduction megathrust. Geophys. Res. Lett. 39, L23301. http://dx.doi.org/10.1029/2012GL053793.
Kodaira, S., Iidaka, T., Kato, A., Park, J.O., Iwasaki, T., Kaneda, Y., 2004. High pore fluid pressure may cause silent slip in the Nankai Trough. Science 304, 1295–1298.
Kukowski, N., et al., 2001. Morphotectonics and mechanics of the central Makran accretionary wedge off Pakistan. Mar. Geol. 173, 1–19.
Lallemand, S.E., Schnurle, P., Malavielle, J., 1994. Coulomb theory applied to accretionary and nonaccretionary wedges: Possible causes for tectonic erosion and/or frontal accretion. J. Geophys. Res. 99, 12033–12055.
Larson, K.M., Kostoglodov, V., Lowry, A., Hutton, W., Sanchez, O., Hudnut, K., Suarez, G., 2004. Crustal deformation measurements in Guerrero, Mexico. J. Geophys. Res. 109, B04409. http://dx.doi.org/10.1029/2003JB002843.
Leitner, B., Eberhart-Phillips, D., Anderson, H., Nabelek, J.L., 2001. A focussed look at the Alpine fault, New Zealand: seismicity, focal mechanisms and stress observations. J. Geophys. Res. 106, 2193–2220.
Lewis, K.B., Marshall, B.A., 1996. Seep faunas and other indicators of methane-rich dewatering on the New Zealand convergent margins. New Zeal. J. Geol. Geophys. 39, 181–200.
Lewis, K.B., Collot, J.-Y., Davy, B.W., Delteil, J., Lallemand, S.E., Uruski, C.I., GeodyNZ Team, 1997. North Hikurangi GeodyNZ swath maps: Depth, texture and geological interpretation. NIWA Chart Misc. Ser., vol. 72. Natl. Inst. of Water and Atmos. Res., Wellington.
Lewis, K.B., Collot, J.-Y., Lallemand, S.E., 1998. The dammed Hikurangi Trough: a channel-fed trench blocked by subducting seamounts and their wake avalanches (New Zealand–France GeodyNZ Project). Basin Res. 10, 441–468.
Ludwig, W.J., Nafe, J.E., Drake, C.L., 1970. Seismic refraction. In: Maxwell, A.E. (Ed.), The Sea, vol. 4. Wiley-Interscience, New York, pp. 53–84.
MacKinnon, T.C., 1983. Origin of the Torlesse Terrane and coeval rocks, South Island, New Zealand. Geol. Soc. Am. Bull. 94, 967–985.
Magara, K., 1978. Compaction and Fluid Migration, vol. 9. Elsevier Science.
Magee, M.E., Zoback, M.D., 1993. Evidence for a weak interplate thrust fault along the northern Japan subduction zone and implications for the mechanics of thrust faulting and fluid expulsion. Geology 21 (9), 809–812.

Matmon, D., Bekins, B.A., 2006. Hydromechanics of a high taper angle, low-permeability prism: a case study from Peru. J. Geophys. Res. 111, B07101.
Mavko, G., Mukerji, T., Dvorkin, J., 1998. The Rock Physics Handbook: Tools for Seismic Analysis in Porous Media. Cambridge University Press, UK. 329 pp.
Mazengarb, C., 1984. The Fernside fault: An active normal fault, Raukumara Peninsula, New Zealand. Rec. New Zeal. Geol. Surv. 3, 98–103.
McCaffrey, R., Wallace, L., Beavan, J., 2008. Slow slip and frictional transition at low temperature at the Hikurangi subduction zone. Nat. Geosci. 1, 316–320.
McIntosh, K.D., Sen, M.R., 2000. Geophysical evidence for dewatering and deformation processes in the ODP Leg 170 area offshore Costa-Rica. Earth Planet. Sci. Lett. 178, 125–138.
Moore, D.E., Rymer, M.J., 2007. Talc-bearing serpentinite and the creeping section of the San Andreas fault. Nature 448 (7155), 795–797.
Moore, J.C., Tobin, H.J., 1997. Estimated fluid pressures of the Barbados accretionary prism and adjacent sediments. In: Shipley, T.H., et al. (Eds.), Proceedings of the Ocean Drilling Program. In: Scientific Results, vol. 156. Ocean Drilling Program, College Station, Texas, pp. 229–238.
Moore, J.C., et al., 1982. Offscraping and underthrusting of sediment at the deformation front of the Barbados Ridge: Deep Sea Drilling Project leg 78A. Geol. Soc. Am. Bull. 93, 1065–1077.
Moore, G.F., et al., 2001. New insights into deformation and fluid flow processes in the Nankai Trough accretionary prism: Results of Ocean Drilling Program Leg 190. Geochem. Geophys. Geosyst. 2. http://dx.doi.org/10.1029/2001GC000166.
Mortimer, N., 2004. New Zealand's geological foundations. Gondwana Res. 7, 261–272. http://dx.doi.org/10.1016/S1342-937X(05)70324-5.
Multiwave, 2005. 05CM 2D seismic survey, offshore east coast – North Island. Open File Petrol. Rep., vol. 3136. Minist. of Econ. Dev., Wellington, NZ, pp. 1–280.
Nafe, J.E., Drake, C.L., 1957. Variation with depth in shallow and deep water marine sediments of porosity, density and the velocities of compressional shear waves. Geophysics 22 (3), 523–552. http://dx.doi.org/10.1190/1.1438386.
Nicol, A., Wallace, L., 2007. Temporal stability of deformation rates: Comparison of geological and geodetic observations, Hikurangi subduction margin, New Zealand. Earth Planet. Sci. Lett. 258, 397–413.
Nicol, A., Mazengarb, C., Chanier, F., Rait, G., Uruski, C., Wallace, L., 2007. Tectonic evolution of the Hikurangi subduction margin, New Zealand, since Oligocene. Tectonics 26. http://dx.doi.org/10.1029/2006TC002090.
Nur, A., Mavko, G., Dvorkin, J., Galmudi, D., 1998. Critical porosity: a key to relating physical properties to porosity in rocks. Lead. Edge 17, 357–362.
Obara, K., Hirose, H., Yamamizu, F., Kasahara, K., 2004. Episodic slow slip events accompanied by non-volcanic tremors in southwest Japan subduction zone. Geophys. Res. Lett. 31, L23602.
Ohta, Y., Kimata, F., Sagiya, T., 2004. Reexamination of the interplate coupling in the Tokai region, central Japan, based on the GPS data in 1997–2002. Geophys. Res. Lett. 31, L24604.
Ohta, Y., Freymueller, J.T., Hreinsdottir, S., Suito, H., 2006. A large slow slip event and the depth of the seismogenic zone in the south central Alaska subduction zone. Earth Planet. Sci. Lett. 247, 108–116.
Park, J.-O., et al., 2010. A low-velocity zone with weak reflectivity along the Nankai subduction zone. Geology 38, 283–286. http://dx.doi.org/10.1130/G30205.1.
Peacock, S.M., 2009. Thermal and metamorphic environment of subduction zone episodic tremor and slip. J. Geophys. Res. 114, B00A07. http://dx.doi.org/10.1029/2008JB005978.
Pedley, K.L., Barnes, P.M., Pettinga, J.R., Lewis, K.B., 2010. Seafloor structural geomorphic evolution of the accretionary frontal wedge in response to seamount subduction, Poverty Indentation, New Zealand. Mar. Geol. 270, 119–138.
Peng, Z., Gomberg, J., 2010. An integrated perspective of the continuum between earthquake and slow slip phenomena. Nat. Geosci. 3, 599–607.
Raymer, L.L., Hunt, E.R., Gardner, J.S., 1980. An improved sonic transit time-to-porosity transform. In: Trans. SPWLA 21st Annu. Log. Symp., P1–P13.
Reuss, A., 1929. Berechnung der Fliessgrenzen von Mischkristallen auf Grund der Plastizitatsbedingging fur Einkristalle. Z. Angew. Math. Mech. 9, 49–58.
Reyners, M., Eberhart-Phillips, D., 2009. Small earthquakes provide insight into plate coupling and fluid distribution in the Hikurangi subduction zone, New Zealand. Earth Planet. Sci. Lett. 282 (1–4), 299–305. http://dx.doi.org/10.1016/j.epsl.2009.03.034.
Reyners, M., McGinty, P., 1999. Shallow subduction tectonics in the Raukumara Peninsula, New Zealand, as illuminated by earthquake focal mechanisms. J. Geophys. Res., Solid Earth 104, 3025–3034.
Reyners, M., Eberhart-Phillips, D., Stuart, G., 1999. A three-dimensional image of shallow subduction: Crustal structure of the Raukumara Peninsula, New Zealand. Geophys. J. Int. 137 (3), 873–890. http://dx.doi.org/10.1046/j.1365-246x.1999.00842.x.
Reyners, M., Eberhart-Phillips, D., Stuart, G., Nishimura, Y., 2006. Imaging subduction from the trench to 300 km depth beneath the central North Island, New Zealand, with V_p and V_p/V_s. Geophys. J. Int. 165, 565–583.
Rubey, W.W., Hubbert, M.K., 1959. Over-thrust belt in geosynclinal area of western Wyoming in light of fluid-pressure hypothesis, 2: Role of fluid pressure in mechanics of overthrust faulting. Geol. Soc. Am. Bull. 70, 167–205.
Rubinstein, J.L., Shelly, D.R., Ellsworth, W.L., 2010. Non-volcanic tremor: a window into the roots of fault zone. In: Cloetingh, S., Negendank, J. (Eds.), New Frontiers in Integrated Solid Earth Sciences. Springer, Netherlands, pp. 287–314.
Saffer, D.M., 2003. Pore pressure development and progressive dewatering in underthrust sediments at the Costa Rican subduction margin: Comparison with northern Barbados and Nankai. J. Geophys. Res. 108 (B5), 2261. http://dx.doi.org/10.1029/2002JB001787.
Saffer, D.M., Bekins, B.A., 1998. Episodic fluid flow in the Nankai accretionary complex: Timescale, geochemistry, flow rates, and fluid budget. J. Geophys. Res. 103, 30351–30371.
Saffer, D.M., Bekins, B.A., 2006. An evaluation of factors influencing pore pressure in accretionary complexes: Implications for taper angle and wedge mechanics. J. Geophys. Res. 111, B04101. http://dx.doi.org/10.1029/2005JB003990.
Saffer, D.M., Marone, C., 2003. Comparison of smectite and illite-rich gouge frictional properties: application to the updip limit of the seismogenic zone along subduction megathrusts. Earth Planet. Sci. Lett. 215 (1), 219–235.
Saffer, D.M., Tobin, H.J., 2011. Hydrogeology and mechanics of subduction zone forearcs: fluid flow and pore pressure. Annu. Rev. Earth Planet. Sci. 2011 (39), 157–186.
Saffer, D., et al., 2009. NanTroSEIZE Stage 2: NanTroSEIZE riser/riserless observatory. Integr. Ocean Drill. Program Prelim. Rep. 319. http://dx.doi.org/10.2204/iodp.pr.319.2009.
Scherwath, M., et al., 2010. Fore arc deformation and underplating at the northern Hikurangi margin, New Zealand. J. Geophys. Res. 115, B06408. http://dx.doi.org/10.1029/2009JB006645.
Scholz, C.H., 1998. Earthquakes and friction laws. Nature 391, 37–42. http://dx.doi.org/10.1038/34097.
Schwartz, S.Y., Rokosky, J.M., 2007. Slow slip events and seismic tremor at circum-pacific subduction zones. Rev. Geophys. 45, RG3004. http://dx.doi.org/10.1029/2006RG000208.
Sclater, J.G., Christie, P.A.F., 1980. Continental stretching: An explanation of the post-Mid-Cretaceous subsidence of the central North Sea Basin. J. Geophys. Res. 85 (B7), 3711–3739. http://dx.doi.org/10.1029/JB085iB07p03711.
Screaton, E.J., Wuthritch, D.R., Dreiss, S.J., 1990. Permeabilities, fluid pressures, and flow rates in the Barbados Ridge complex. J. Geophys. Res. 95, 8997–9007.
Sibson, R.H., 1982. Fault zone models, heat-flow, and the depth distribution of earthquakes in the continental crust of the United States. Bull. Seismol. Soc. Am. 72 (1), 151–163.
Sibson, R.H., Rowland, J.V., 2003. Stress, fluid pressure and structural permeability in seismogenic crust, North Island, New Zealand. Geophys. J. Int. 154, 584–594. http://dx.doi.org/10.1046/j.1365-246X.2003.01965.x.
Sugioka, H., Okamoto, T., Nakamura, T., Ishihara, Y., Ito, A., Obana, K., Kinoshita, M., Nakahigashi, K., Shinohara, M., Fukao, Y., 2012. Tsunamigenic potential of the shallow subduction plate boundary inferred from slow seismic slip. Nat. Geosci. 5, 414–418. http://dx.doi.org/10.1038/ngeo1466.
Swarbrick, R.E., 1997. Pressure compartments and their interdependence on overpressure mechanisms: examples from the North Sea. Am. Assoc. Pet. Geol. Bull. 81 (8), 1415.
Takei, Y., 2002. Effect of pore geometry on V_p/V_s: From equilibrium geometry to crack. J. Geophys. Res. 107 (B2), 2043. http://dx.doi.org/10.1029/2001JB000522.
Terzaghi, K., Peck, R.B., 1948. Soil Mechanics in Engineering Practice. Wiley, New York.
Thornley, S., 1996. Neogene tectonics of Raukumara Peninsula, northern Hikurangi Margin, New Zealand. Ph.D. thesis. Victoria Univ. of Wellington, New Zealand.
Tobin, H.J., Saffer, D.M., 2009. Elevated fluid pressure and extreme mechanical weakness of a plate boundary thrust, Nankai Trough subduction zone. Geology 37, 679–682. http://dx.doi.org/10.1130/G25752A.1.
Tobin, H., et al., 2009. Expedition 314 summary. In: NanTroSEIZE Stage 1: Investigations of Seismogenesis. Nankai Trough, Japan. In: Proc. Integr. Ocean Drill. Program, vol. 314/315/316.
Toksöz, M.N., Cheng, C.H., Timur, A., 1976. Velocities of seismic waves in porous rocks. Geophysics 41, 621–645.
Townend, J., Sherburn, S., Arnold, R., Boese, C., Woods, L., 2012. Three-dimensional variations in present day tectonic stress along the Australia–Pacific plate boundary in New Zealand. Earth Planet. Sci. Lett.. http://dx.doi.org/10.1016/j.epsl.2012.08.003.
Tsuji, T., Tokuyama, H., Costa Pisani, P., Moore, G., 2008. Effective stress and pore pressure in the Nankai accretionary prism off the Muroto Peninsula, southwestern Japan. J. Geophys. Res., Solid Earth 113 (B11), B11401.
van Avendonk, H.J.A., Holbrook, W.S., Okaya, D., Austin, J.K., Davey, F., Stern, T., 2004. Continental crust under compression: A seismic refraction study of South Island Geophysical Transect I, South Island, New Zealand. J. Geophys. Res. 109, B06302. http://dx.doi.org/10.1029/2003JB002790.
von Huene, R., Lee, H., 1982. The possible significance of pore fluid pressures in subduction zones. In: Watkins, S., Drake, C.L. (Eds.), Studies in Continental Margin Geology: American Association of Petroleum Geologists Memoir 34, 781–792.
Wallace, L.M., Beavan, R.J., 2006. A large slow slip event on the central Hikurangi subduction interface beneath the Manawatu region, North Island, New Zealand. Geophys. Res. Lett. 33, L11301. http://dx.doi.org/10.1029/2006GL026009.
Wallace, L.M., Beavan, J., 2010. Diverse slow slip behavior at the Hikurangi subduction margin, New Zealand. J. Geophys. Res., Solid Earth 115.

Wallace, L.M., Beavan, J., McCaffrey, R., Darby, D., 2004. Subduction zone coupling and tectonic block rotations in the North Island, New Zealand. J. Geophys. Res. 109, B12406. http://dx.doi.org/10.1029/2004JB003241.

Wallace, L.M., et al., 2009. Characterizing the seismogenic zone of a major plate boundary subduction thrust: Hikurangi Margin, New Zealand. Geochem. Geophys. Geosyst. 10, Q10006. http://dx.doi.org/10.1029/2009GC002610.

Wallace, L.M., Beavan, J., Bannister, S., Williams, C., 2012. Simultaneous long-term and short-term slow slip events at the Hikurangi subduction margin, New Zealand: Implications for processes that control slow slip event occurrence, duration, and migration. J. Geophys. Res. 117, B11402. http://dx.doi.org/10.1029/2012JB009489.

Wang, K., 1994. Kinematics of dewatering accretionary prisms. J. Geophys. Res. 99, 4429–4438.

Wang, K., Hu, Y., He, J., 2012. Deformation cycles of subduction earthquakes in a viscoelastic Earth. Nature. http://dx.doi.org/10.1038/nature11032.

Wech, A.G., Creager, K.C., 2011. A continuum of stress, strength and slip in the Cascadia transition zone. Nat. Geosci. 4, 624–628.

Williams, C.A., Eberhart-Phillips, D., Bannister, D., Barker, D., Henrys, S., Reyners, M., Sutherland, R., in press. Revised Interface Geometry for the Hikurangi Subduction Zone, New Zealand. Seismol. Res. Lett..

Wright, I.C., Parson, L.M., Gamble, J.A., 1996. Evolution and interaction of migrating cross-arc volcanism and backarc rifting: An example from the southern Havre Trough (35°200–37°S). J. Geophys. Res. 101, 22071–22086. http://dx.doi.org/10.1029/96JB01761.

Wright, I.C., Worthington, T.J., Gamble, J.A., 2006. New multibeam mapping and geochemistry of the 30°–35°S sector, and overview, of southern Kermadec arc volcanism. J. Volcanol. Geotherm. Res. 149, 263–296. http://dx.doi.org/10.1016/j.jvolgeores.2005.03.021.

Wyllie, M.R.J., Gregory, A.R., Gardner, G.H.F., 1956. Elastic wave velocities in heterogeneous and porous media. Geophysics 21, 41–70.